

**FABRICATION OF THREE DIMENSIONAL
(3D)-PRINTED ELECTRODES-BASED
THERMOPLASTIC CARBON NANOMATERIALS
FOR ELECTROCHEMICAL BREAST CANCER
DNA BIOSENSOR**

MUHAMAD HUZAIFAH BIN OMAR

UNIVERSITI SAINS MALAYSIA

2023

**FABRICATION OF THREE DIMENSIONAL
(3D)-PRINTED ELECTRODES-BASED
THERMOPLASTIC CARBON NANOMATERIALS
FOR ELECTROCHEMICAL BREAST CANCER
DNA BIOSENSOR**

by

MUHAMAD HUZAIFAH BIN OMAR

**Thesis submitted in fulfilment of the requirements
for the degree of
Master of Science**

August 2023

ACKNOWLEDGEMENT

First and foremost, I would like to express my utmost appreciation to my supervisor, Dr. Hairul Hisham Hamzah, for his guidance, assistance, insight and encouragement throughout my master's programme. I would also like to express my deepest gratitude to Jabatan Perkhidmatan Awam (JPA) for Biasiswa Yang Di Pertuan Agong (BYDPA) scholarships and Fundamental Research Grant Scheme (FRGS) grant (230.PKIMIA.6711919) for the financial support that allowed me to complete my master's study. Furthermore, I also would like to express my sincere gratitude to Professor Bhavik Anil Patel, University of Brighton, UK, for providing some ideas for this research. Also, thanks to Dr. Mohd Nadhir Abdul Wahab, Prof. Dr. Khairunisak Abdul Razak, and Mrs. Nor Dyana Zakaria for guidance, advice, and encouragement that helped me to complete my research. I would also like to acknowledge Universiti Sains Malaysia (USM) for providing the environment equipped with facilities and instruments. Special gratitude to all of the academic and non-academic personnel at the School of Chemical Sciences who assisted me throughout my studies. Last but not least, I would like to express my deepest appreciation to my parents for their endless love, encouragement, understanding, and belief in me. All of my achievements would be impossible without their presence in my life.

TABLE OF CONTENTS

ACKNOWLEDGEMENT.....	ii
TABLE OF CONTENTS.....	iii
LIST OF TABLES.....	vii
LIST OF FIGURES.....	viii
LIST OF SYMBOLS AND ABBREVIATIONS.....	xv
ABSTRAK.....	xxi
ABSTRACT.....	xxiii
CHAPTER 1 INTRODUCTION.....	1
1.1 Background of the study.....	1
1.2 Problem statement.....	8
1.3 Research objectives.....	10
1.4 Research overview.....	10
CHAPTER 2 LITERATURE REVIEW.....	13
2.1 The effect of printing on the electrodes' electrochemical behaviour.....	13
2.2 The effect of carbon nanomaterials contents on the 3D-printed electrodes.....	16
2.3 Chemical and electrochemical activation studies on 3D-printed electrodes.....	19
2.4 Application of 3D-printed electrodes as electrochemical sensors...	25
2.5 Application of 3D-printed electrodes as electrochemical biosensors.....	28
2.6 Electrochemical biosensors for the detection of BRCA1.....	34
2.7 Established clinical methods for early breast cancer diagnosis.....	42

CHAPTER 3	MATERIALS AND EXPERIMENTALS.....	47
3.1	Chemicals and materials.....	47
3.2	Printing and fabrication of 3D PLA/CF and 3D PLA/G electrodes.	48
3.3	Chemical and electrochemical activations of the 3D-printed electrodes.....	49
3.4	Characterisation of 3D-printed electrodes.....	50
3.4.1	Field emission scanning electron microscopy (FESEM) analyses.....	50
3.4.2	Electrochemical characterisation.....	50
3.4.2(a)	Cyclic voltammetry (CV).....	51
3.4.2(b)	Differential pulse voltammetry (DPV).....	51
3.4.2(c)	Scan rate studies.....	52
3.4.2(d)	Electrochemical impedance spectroscopy (EIS)	52
3.5	Fabrication of BRCA1 DNA based 3D PLA/G biosensor.....	53
3.5.1	Printing and fabrication of 3D PLA/G electrode.....	53
3.5.2	Preparation of amine linker electrografting solution.....	54
3.5.3	Electrografting of amine linker onto 3D PLA/G electrode surface.....	54
3.5.4	Immobilisation of BRCA1 ssDNA probe on the surface of the electrode.....	54
3.6	Characterisation and evaluation of 3D PLA/G BRCA1 biosensor...	55
3.6.1	Characterisation of electrografted 3D PLA/G electrode....	55
3.6.2	The evaluation of 3D PLA/G electrode following ssDNA probe immobilisation.....	56
3.6.3	X-ray photoelectron spectroscopy (XPS).....	56
3.6.4	Hybridisation of the immobilised ssDNA probes.....	57
3.7	Data analyses.....	57

CHAPTER 4	A NEW ELECTROCHEMICAL TREATMENT UTILISING DPV TECHNIQUE FOR ENHANCING THE ELECTROCHEMICAL PERFORMANCES OF PLA/CARBON FIBER 3D-PRINTED ELECTRODES.....	58
4.1	Results and discussion.....	58
4.1.1	CV and DPV studies of 3D PLA/CF electrodes.....	59
4.1.2	CV capacitive current study on 3D PLA/CF electrodes....	65
4.1.3	FESEM analyses of 3D PLA/CF electrodes.....	66
4.1.4	Studies on the CV scan rate of 3D PLA/CF electrodes.....	67
4.1.5	CV and EIS analyses of 3D PLA/CF electrodes in ferri/ferrocyanide solution.....	70
4.2	Summary.....	75
CHAPTER 5	THE EFFECT OF DPV ELECTROCHEMICAL TREATMENT IN RUHEX AND NAOH SOLUTIONS ON 3D - PRINTED PLA / GRAPHENE ELECTRODES.....	76
5.1	Results and discussion.....	76
5.1.1	CV characterisation.....	77
5.1.2	DPV characterisation.....	83
5.1.3	FESEM analyses.....	85
5.1.4	Effect of scan rate on 3D PLA/G electrode.....	87
5.1.5	EIS characterisation.....	90
5.2	Summary.....	96
CHAPTER 6	3D-PRINTED ELECTRODE AS MODIFIED ELECTRODE TO STUDY ELECTROCHEMICAL DNA BIOSENSOR-BASED LABELLED SYSTEM FOR BRCA1 GENE.....	98
6.1	Results and discussion.....	98

6.1.1	Electrografting of amine linker onto the 3D PLA/G electrode surfaces.....	98
6.1.2	Electrochemical characterisation of the immobilised ssDNA molecular probe on the 3D PLA/G electrode.....	102
6.1.3	X-ray photoelectron spectroscopy (XPS) analyses.....	108
6.1.4	Evaluation of ssDNA/3D PLA/G modified electrodes on detection BRCA1 gene ssDNA sequence.....	114
6.2	Summary.....	120
CHAPTER 7 CONCLUSION AND RECOMMENDATIONS		121
7.1	Conclusion.....	121
7.2	Recommendation and future works.....	123
REFERENCES.....		125
APPENDICES		
LIST OF PUBLICATION		

LIST OF TABLES

		Page
Table 2.1	Summary of activation methods of the 3D-printed electrodes with their respective applications.....	23
Table 2.2	Summary of fabricated BRCA1 electrochemical biosensor based on conventional and screen-printed electrodes.....	40
Table 3.1	ssDNAs sequences used in the study.....	48
Table 4.1	Computed D values for the 3D PLA/CF electrode before and after DPV-RuHex electrochemical treatment.....	70
Table 5.1	The i_{pa} values from CVs of untreated 3D PLA/G electrodes before background subtraction.....	78
Table 5.2	Calculated D values for 3D PLA/G electrode before and after both DPV electrochemical treatments.....	90
Table 6.1	Atomic composition of 3D PLA/G electrode before, grafted, and after ssDNA probe immobilisation.....	108
Table 6.2	Bonding composition of 3D PLA/G electrode before, grafted, and after ssDNA probe immobilisation at their respective binding energy.....	111

LIST OF FIGURES

		Page
Figure 1.1	Dr. Hideo Kodama is one of the pioneers in 3D printing.....	1
Figure 1.2	Creality CR-6 SE 3D printer is an example of an FDM 3D printer.....	2
Figure 1.3	The common basic structure of FDM 3D printer.....	3
Figure 1.4	Schematic illustration of the FDM 3D printing process.....	4
Figure 1.5	Common thermoplastic PLA and ABS filaments are used in the 3D printing process.....	5
Figure 2.1	3D PLA/CB electrodes were printed in different thicknesses of 0.1 to 0.4 mm with horizontal and vertical orientations [67].....	15
Figure 2.2	Preparation of TPI/CNT filament containing different wt% of CNT [68].....	17
Figure 2.3	Resistivity against NG content plot, demonstrating effective percolation for NG content more than 20% which results in higher conductivity [69].....	18
Figure 2.4	(A) and (B) showing cyclic voltammograms in $[\text{Fe}(\text{CN})_6]^{3-/4-}$ solution of 3D PLA/G electrodes after chemically activated with different solvents [35].....	20
Figure 2.5	Preparation of 3D-printed electrodes with electrochemical activation and chemical activation using sodium borohydride. The cyclic voltammograms indicated the electrodes' redox activity before and after activation in $[\text{Fe}(\text{CN})_6]^{3-/4-}$ solution [72].....	22
Figure 2.6	Cyclic voltammograms of the 3D-printed nanocarbon electrodes before and after activating with DMF and sodium borohydride (NaBH_4) solutions [72].....	22
Figure 2.7	Preparation of 3D-printed PLA/G electrodes and their pre-treatment before using them for ZEA detection [32].....	26
Figure 2.8	Schematic diagram summarising the research done for detecting metals in urine and saliva samples [36].....	27

Figure 2.9	Schematic diagram of the fabrication of 3D PLA/G biosensor for the detection of H ₂ O ₂ : (A) 3D PLA/G electrode printing, (B) chemical and electrochemical activation of the electrode, (C) immobilisation of HRP enzyme on the electrode, and (D) immobilisation of HRP enzyme on the AuNPs-modified electrode. (E) and (F) indicates the mechanism for the detection of H ₂ O ₂ [33].....	29
Figure 2.10	Schematic diagram showing the fabrication of the immunosensor, step by step [80].....	30
Figure 2.11	Schematic diagram illustrating the fabrication of 3D PLA/G biosensor for detection of 1-naphthol [82].....	32
Figure 2.12	Schematic diagram showing the fabrication step of 3D PLA/G biosensor after activation for detection of catechol: (A) DHP and tyrosinase mixing, (B) immobilisation of the mixture via drop casting, (C) formation of the film on electrode's surface, and (D) the electrochemical detection of catechol [83].....	34
Figure 2.13	Schematic diagrams showing (A) formation of peptide monolayer on the gold electrode and (B) fabrication and detection of DNA electrochemical biosensor [85].....	36
Figure 2.14	Schematic diagrams showing the fabrication of BRCA1-SPCE biosensor [87].....	38
Figure 2.15	Breast MRI machine for breast cancer screening [106].....	45
Figure 3.1	Image of the fabricated electrodes: (A) 3D PLA/CF electrode and (B) 3D PLA/G electrode.....	49
Figure 3.2	3D PLA/G electrode used in Chapter 6.....	53
Figure 3.3	Schematic representation of the immobilisation of the BRCA1 ssDNA probe on the 3D PLA/G electrode surface in two steps. Step 1 : electrografting of 6-aminohexanoic acid on the surface of the electrode using the CV technique, and Step 2 : immobilisation of BRCA1 ssDNA probe on the surface of the electrode by covalent bonding of carboxyl group of the grafted amine linker and the amine group of the ssDNA probe. <i>Conditions</i> : (a) CV conducted between a potential of 0.6 to 1.8 V vs. Ag/AgCl for 4 cycles at a scan rate of 100 mV s ⁻¹ in 15 mM 6-aminohexanoic acid prepared in KCl/ethanol solution; (b) ssDNA probe solution was drop cast onto electrode surface in the presence of NHS and EDC (1:1).....	55

Figure 4.1	(A) Cyclic voltammograms and (B) differential pulse voltammograms of 3D PLA/CF electrodes in 3 mM RuHex solution for before, control, and after DPV-RuHex electrochemical treatment.....	59
Figure 4.2	(A) Anodic peak currents (i_{pa}), (B) cathodic peak currents (i_{pc}), and (C) DPV peak currents of 3D PLA/CF electrodes before, control, and after DPV-RuHex electrochemical treatment. Statistical analyses were performed using the post hoc Tukey test. Data are shown as mean \pm SD; n = 3; and *, **, and *** denote $p < 0.05$, $p < 0.01$, and $p < 0.001$, respectively.....	61
Figure 4.3	The DPV current generated by the 3D PLA/CF electrode following DPV electrochemical treatment in RuHex and phosphate buffer solutions, respectively.....	63
Figure 4.4	Cyclic voltammograms showing capacitive currents of the 3D PLA/CF electrodes before, control, and after DPV-RuHex electrochemical treatment at scan rate of 100 mV s^{-1} in 0.1 M PB solution.....	65
Figure 4.5	The surface morphologies of 3D PLA/CF electrodes for (A) freshly printed, (B) after chemical activation in DMF solution, and (C) after DPV electrochemical treatment in RuHex solution. The FESEM images were taken at 100x magnification. The blue and yellow circles indicate the changes observed on the electrodes' surfaces following DMF chemical activation and DPV-RuHex treatment, respectively.....	66
Figure 4.6	Cyclic voltammograms of 3D PLA/CF electrodes at various scan rates from 10 to 250 mV s^{-1} in 3 mM RuHex solution for (A) untreated electrodes and (B) DPV-RuHex treated electrodes. (C) The plot of i_{pa} and i_{pc} of 3D PLA/CF electrodes versus square root of scan rate ($v^{1/2}$) before (red) and after (blue) DPV electrochemical treatment in RuHex...	68
Figure 4.7	(A) Cyclic voltammograms of 3D PLA/CF electrodes before and after DPV-RuHex treatment at a scan rate of 100 mV s^{-1} in a solution containing 10 mM $[\text{Fe}(\text{CN})_6]^{3-/4-}$ with 0.1 M KCl as supporting electrolyte. (B) Nyquist plots, and (C) Bode plots of 3D PLA/CF electrodes before and after DPV-RuHex treatment recorded at a 5 mV amplitude over a 100 kHz to 0.1 Hz frequency range in 10 mM $[\text{Fe}(\text{CN})_6]^{3-/4-}$ with 0.1 M KCl as supporting electrolyte.....	71

Figure 4.8	Suggested equivalent circuit model used in the convergent fitting of the Nyquist and Bode plots from EIS measurements for 3D PLA/CF electrode before and after DPV treatment, where RE is the reference electrode, R_s is the solution resistance, R_{ct} is the charge-transfer resistance, and CPE is the constant phase element.....	73
Figure 4.9	(A) Solution resistance (R_s), (B) charge transfer resistance (R_{ct}), and (C) heterogeneous electron transfer rate constant (k^o) values, for 3D PLA/CF electrodes before and after DPV electrochemical treatment in RuHex. Statistical analyses were performed using the unpaired Student's t-test. Data are shown as mean \pm SD; n = 3; ** denotes $p < 0.01$, and *** denotes $p < 0.001$	73
Figure 5.1	Cyclic voltammograms of 3D PLA/G electrodes for before and after DPV-RuHex treatment (A), and for before and after DPV-NaOH treatment (B), in 3 mM RuHex solution between the potential of -0.5 to -0.03 V vs. SCE, at a scan rate of 100 mV s ⁻¹ for 5 cycles.....	77
Figure 5.2	(A) Anodic peak currents (i_{pa}) of different 3D PLA/G electrodes from CV after background subtraction. (B) i_{pa} of the 3D PLA/G electrodes before (1) and after (2) DPV-RuHex and DPV-NaOH treatments. (C) i_{pa} changes (Δi_{pa}) of 3D PLA/G electrodes before and after DPV-RuHex and DPV-NaOH treatments. (D) Comparison of Δi_{pa} produced by 3D PLA/G electrodes for both DPV treatments. Statistical analysis was performed by using the unpaired Student's t-test. Data are shown as mean \pm SD; n = 3; and ** denotes $p < 0.01$	79
Figure 5.3	(A) Cathodic peak currents (i_{pc}) of different 3D PLA/G electrodes from CV after background subtraction. (B) i_{pc} of the 3D PLA/G electrodes before (1) and after (2) DPV-RuHex and DPV-NaOH treatments. (C) i_{pc} changes (Δi_{pc}) of 3D PLA/G electrodes before and after DPV-RuHex and DPV-NaOH electrochemical treatments. (D) Comparison of Δi_{pc} produced by 3D PLA/G electrodes for both DPV treatments. Statistical analysis was performed by using the unpaired Student's t-test. Data are shown as mean \pm SD; n = 3.....	80

Figure 5.4	(A) Peak separation ($E_{pa} - E_{pc} / \Delta E_p$) of different 3D PLA/G electrodes before (1) and after (2) DPV-RuHex and DPV-NaOH electrochemical treatments. Comparison of peak separation values of the 3D PLA/G electrodes before treatment and after DPV-RuHex treatment (B), before treatment and after DPV-NaOH treatment (C), and for both DPV treatments (D). Statistical analyses were performed using the unpaired Student's t-test. Data are shown as mean \pm SD; n = 3; and * denotes $p < 0.05$	81
Figure 5.5	Differential pulse voltammograms of 3D PLA/G electrodes for before and after DPV-RuHex treatment (A), and for before and after DPV-NaOH treatment (B), in 3 mM RuHex solution between -0.7 to 0.0 V vs. SCE at a scan rate of 10 $mV s^{-1}$	83
Figure 5.6	(A) Anodic peak currents (i_{pa}) of different 3D PLA/G electrodes from DPV after background subtraction. (B) i_{pa} of the 3D PLA/G electrodes before (1) and after (2) DPV-RuHex and DPV-NaOH treatments. (C) i_{pa} changes (Δi_{pa}) of 3D PLA/G electrodes before and after DPV-RuHex and DPV-NaOH treatments. (D) Comparison of DPV Δi_{pa} produced by 3D PLA/G electrodes for both DPV treatments. Statistical analysis was performed by using the unpaired Student's t-test. Data are shown as mean \pm SD; n = 3.....	84
Figure 5.7	The surface morphologies of 3D PLA/G electrodes for (A) before and (B) after DPV-RuHex treatment, and for (C) before and (D) after DPV-NaOH treatment. The FESEM analyses were conducted at 100x magnification. The yellow circles indicate the changes observed on the electrodes' surfaces following both DPV treatments.....	86
Figure 5.8	Cyclic voltammograms of 3D PLA/G electrodes for before (A) and after DPV-RuHex treatment (B), and for before (C) and after DPV-NaOH treatment (D), at different scan rates between 10 - 250 $mV s^{-1}$ in 3 mM RuHex solution.....	88
Figure 5.9	Plots of anodic (i_{pa}) and cathodic (i_{pc}) peak currents against the square root of scan rate ($v^{1/2}$) for 3D PLA/G electrodes before and after (A) DPV-RuHex treatment and (B) DPV-NaOH treatment.....	89
Figure 5.10	Nyquist plots of 3D PLA/G electrodes before and after DPV-RuHex treatment (A), and before and after DPV-NaOH treatment (B). Bode plots of 3D PLA/G electrodes before and after DPV-RuHex treatment (C), and before and after DPV-NaOH treatment (D). The EIS measurements were conducted in 10 mM $[Fe(CN)_6]^{3-/4-}$ at an amplitude of 5 mV with a frequency range of 100 kHz to 0.1 Hz.....	91

Figure 5.11	(A) and (B) showing suggested equivalent circuit models used in the convergent fitting of the Nyquist and Bode plots from EIS measurements for 3D PLA/G electrodes before and after both DPV treatments, where RE is the reference electrode, R_s is the solution resistance, C_{dl} is the double-layer capacitance, R_{ct} is the charge-transfer resistance, and CPE is the constant phase element.....	92
Figure 5.12	(A) The charge-transfer resistance (R_{ct}) values and (B) the heterogeneous electron transfer rate constant (k^o) values of 3D PLA/G electrodes before and after both DPV treatments. Statistical analyses were performed using the post hoc Tukey test. Data are shown as mean \pm SD; n = 3; and * denotes $p < 0.05$	93
Figure 5.13	Electrochemical responses produced by the 3D PLA/G electrodes during DPV-RuHex electrochemical treatment (A) and DPV-NaOH electrochemical treatment (B).....	95
Figure 6.1	Electrografting of 15mM 6-aminohexanoic (6-AHC) acid in a mixture of 0.1 M KCl and ethanol onto the surface of 3D PLA/G electrode using the CV method for 4 cycles at a scan rate of 100 mV s ⁻¹	99
Figure 6.2	Electrochemical characterisation of 3D PLA/G electrode before and after the electrografting process: (A) Cyclic voltammograms of 3D PLA/G electrode in 10 mM [Fe(CN) ₆] ^{3-/4-} with 0.1 M KCl as supporting electrolyte for 2 cycles at a scan rate of 100 mV s ⁻¹ . (B) Nyquist plots of 3D PLA/G electrode recorded at a 5 mV amplitude over a 100 kHz to 1 Hz frequency range in 10 mM [Fe(CN) ₆] ^{3-/4-} with 0.1 M KCl as supporting electrolyte. (C) Charge transfer resistance (R_{ct}) values of 3D PLA/G electrode before and after the electrografting process. Statistical analysis was performed using the unpaired Student's t-test. Data are shown as mean \pm SD; n = 3.....	100
Figure 6.3	Suggested equivalent circuit model used in the convergent fitting of the Nyquist plots from EIS measurements for 3D PLA/G electrode before and after electrografting, where RE is the reference electrode, R_s is the solution resistance, C_{dl} is the double-layer capacitance, R_{ct} is the charge-transfer resistance, W is the Warburg impedance, and CPE is the constant phase element.....	101
Figure 6.4	Differential pulse voltammograms of 3D PLA/G electrode for bare, grafted, and after ssDNA immobilisation (probe) in 0.1 M PBS solution.....	103

Figure 6.5	(A) DPV response of ssDNA probe with grafted amine linker and control (without grafted amine linker) 3D PLA/G electrodes in 0.1 M PBS solution. (B) DPV current after background subtraction and (C) Statistical analysis of the obtained DPV current. This analysis was performed using the unpaired Student's t-test. Data are shown as mean \pm SD; n = 3; *** denotes $p < 0.001$	104
Figure 6.6	(A) Differential pulse voltammograms (DPVs) scanned between 0.7 to 1.1 V for bare, control, and ssDNA/3D PLA/G modified electrodes in 0.1 M PBS solution. (B) DPV oxidation current of guanine after background subtraction for control and ssDNA/3D PLA/G modified electrodes. (C) Statistical analysis of the obtained DPV current. This analysis was performed using the unpaired Student's t-test. Data are shown as mean \pm SD; n = 3; *** denotes $p < 0.001$...	106
Figure 6.7	XPS spectra of C1s (A), N1s (B), and O1s (C) for bare, grafted, and ssDNA/3D PLA/G modified electrodes.....	109 - 110
Figure 6.8	(A) Differential pulse voltammograms of ssDNA/3D PLA/G modified electrode showing oxidation peak of labelled ferrocene before (black line), and after hybridisation with 3 μ M target ssDNA (complementary) (blue line) and 3 μ M non-complementary (NC) ssDNA (red line) measured in 0.1 M PBS solution. (B) The oxidation current peak of the labelled ferrocene in (A) after background subtraction.....	115
Figure 6.9	(A) Differential pulse voltammograms for ssDNA/3D PLA/G modified electrode before and after exposure to 0.1 μ M target ssDNA (blue line) and 0.1 μ M NC ssDNA (red line). (B) Ferrocene oxidation peak data in (A) after background subtraction. (C) Statistical analyses of the obtained DPV current by the ssDNA/3D PLA/G modified electrode before and after exposure to target ssDNA (0.1 μ M and 3 μ M) and NC ssDNA (0.1 μ M and 3 μ M). These analyses were performed using the post hoc Tukey test. Data are shown as mean \pm SD; n = 3; *** denotes $p < 0.001$	117

LIST OF SYMBOLS AND ABBREVIATIONS

%	Percentage
°C	Degree Celsius
μ	Micro
μA	Microampere
μg	Microgram
μL	Microlitre
μM	Micromolar
v	Scan rate
Ω	Ohm
θ	Phase angle
3D	Three-dimensional
6-AHC	6-aminohexanoic
A	Geometrical surface area
A	Ampere
ABS	Acrylonitrile butadiene styrene
Ag/AgCl	Silver/silver chloride
at.	Atomic
AuNPs	Gold nanoparticles
BRCA1	Breast cancer 1
BSA	Bovine serum albumin
C	Concentration
CAD	Computer aided design

CB	Carbon black
C_{dl}	Double-layer capacitance
Cd^{2+}	Cadmium (II) ion
CF	Carbon fiber
C_2H_3N	Acetonitrile
$C_6H_{13}NO_2$	6-aminohexanoic acid
C_2H_5OH	Ethanol
cm	Centimetre
CNT	Carbon nanotubes
CPE	Constant phase element
Cu^{2+}	Copper (II) ion
CV	Cyclic voltammetry
D	Diffusion coefficient
DHP	Dihexadecyl phosphate
DMF	Dimethylformamide
DNA	Deoxyribonucleic acid
DPV	Differential pulse voltammetry
$E_{1/2}$	Mid potential
EDC	<i>N</i> -(3-dimethylaminopropyl)- <i>N'</i> -ethylcarbodiimide hydrochloride
EIS	Electrochemical impedance spectroscopy
ΔE_p	Potential peak separation
E_{pa}	Anodic peak potential
E_{pc}	Cathodic peak potential
EPPG	Edge-plane pyrolytic graphite

F	Faradaic constant
FDM	Fused deposition modelling
$[\text{Fe}(\text{CN})_6]^{3-/4-}$	Ferricyanide/ferrocyanide redox pair
FESEM	Field emission scanning electron microscopy
fM	Femtomolar
G	Graphene
g	Gram
GCE	Glassy carbon electrode
gcode	Geometric Code
GE	Gold electrode
h	Hour
HAb	IgG2B antibody
Hg^{2+}	Mercuric (II) ion
HRP	Horseradish peroxidase
HPRS	Horizontal printed rough surface
HPSS	Horizontal printed smooth surface
H_2O_2	Hydrogen peroxide
H_2SO_4	Sulfuric acid
Hz	Hertz
i_{pa}	Anodic peak current
Δi_{pa}	Anodic peak current changes
i_{pc}	Cathodic peak current
Δi_{pc}	Cathodic peak current changes
K	Kelvin
k	Kilo

k°	Heterogeneous electron transfer rate constant
k Ω	Kiloohm
KCl	Potassium chloride
K ₃ Fe(CN) ₆	Potassium ferricyanide
K ₄ Fe(CN) ₆ ·3H ₂ O	Potassium ferrocyanide
kHz	Kilohertz
L	Litre
LOD	Limit of detection
LOQ	Limit of quantification
M	Molar
m	Metre
mA	Milliampere
MCH	6-mercapto-1-hexanol
MES	2-(N-morpholino)ethanesulfonic acid
mg	Milligram
min	Minute
mL	Millilitre
mM	Millimolar
mm	Millimetre
mol	Mole
mV	Millivolt
n	Number of electron
nA	Nanoampere
NaCl	Sodium chloride
Na ₂ HPO ₄	Disodium hydrogen phosphate anhydrous

NaH ₂ PO ₄ ·2H ₂ O	Sodium dihydrogen phosphate dihydrate
NaOH	Sodium hydroxide
NC	Non-complementary
nC	Nanocarbon
NG	Nanographite
NHS	<i>N</i> -hydroxysuccinimide
nM	Nanomolar
Np	Hantavirus Araucaria nucleoprotein
P3CA	Pyrrole – 3 – carboxylic acid
PB	Phosphate buffer
Pb ²⁺	Lead (II) ion
PBS	Phosphate buffer saline
PEDOT	Poly(3,4-ethylenedioxythiophene)
pg	Picogram
PLA	Polylactic acid
PLA/CB	Polylactic acid/carbon black
PLA/CF	Polylactic acid/carbon fiber
PLA/G	Polylactic acid/graphene
pM	Picomolar
PU	Polyurethane
<i>R</i> _{ct}	Charge transfer resistance
<i>R</i> _i	Interface resistance
rGO	Reduced graphene oxide
<i>R</i> _s	Solution resistance
RuHex	Hexaammineruthenium (III) chloride

$[\text{Ru}(\text{NH}_3)_6]^{3+/2+}$	Hexaammineruthenium redox pair
s	Second
SAMs	Self-assembled monolayers
SCE	Saturated calomel electrode
Si	Silicon
SPCE	Screen-printed carbon electrode
SPE	Screen-printed electrode
SPGE	Screen-printed gold electrode
ssDNA	Single-stranded deoxyribonucleic acid
stl	Standard Tessellation Language
Sulfo-NHS	<i>N</i> -Hydroxysulfosuccinimide sodium salt
SWV	Square wave voltammetry
<i>T</i>	Temperature
TE	Tris-ethylenediaminetetraacetic acid
TPI	Thermoplastic polyimide
UV-Vis	Ultraviolet-visible
V	Volt
VP	Vertical printed
vs.	Versus
W	Warburg impedance element
wt.	Weight
XPS	X-ray photoelectron spectroscopy
ZEA	Zearalenone

**FABRIKASI ELEKTROD TERCETAK TIGA DIMENSI (3D) BERASASKAN
BAHAN NANO KARBON TERMOPLASTIK UNTUK PENDERIBIO
ELEKTROKIMIA DNA KANSER PAYUDARA**

ABSTRAK

Pencetakan tiga dimensi (3D) atau pembuatan bahan tambah ialah satu teknologi yang dijangka akan merevolusikan kaedah pembuatan tradisional. Pada masa ini, banyak kajian telah menggunakan teknologi pencetakan 3D untuk menggantikan elektrod konvensional dalam fabrikasi penderia dan penderibio elektrokimia kerana kosnya yang rendah, merupakan sejenis prototaip pantas dan mempunyai reka bentuk yang fleksibel. Tujuan utama kajian ini adalah untuk meneroka potensi elektrod tercetak 3D sebagai penderibio elektrokimia untuk mengesan gen kanser payudara 1 (BRCA1). Bahagian pertama kajian menfokuskan pada prestasi elektrokimia elektrod tercetak 3D berasaskan filamen asid poliaktik/gentian karbon (PLA/CF). Satu rawatan elektrokimia baru menggunakan kaedah voltametri nadi pembezaan (DPV) dalam larutan heksaamineruthenium (III) klorida (RuHex) telah dicadangkan. Pencirian elektrokimia mendedahkan bahawa rawatan elektrokimia DPV-RuHex telah meningkatkan prestasi elektrokimia elektrod 3D PLA/CF dengan ketara. Tambahan pula, foto mikrograf elektron pengimbasan pelepasan medan (FESEM) menunjukkan bahawa lebih banyak lapisan PLA terdegradasi selepas rawatan, yang menyebabkan peningkatan kawasan permukaan elektroaktif elektrod. Bahagian kedua kajian menyelidik kesan rawatan elektrokimia DPV dalam larutan RuHex dan natrium hidroksida (NaOH) terhadap elektrod tercetak 3D PLA/grafin (PLA/G). Hasil daripada analisis elektrokimia mendedahkan tiada

perbezaan yang ketara antara kedua-dua rawatan. Hal ini kerana kedua-dua rawatan ini menjana isyarat pengoksidaan DPV yang sama kuat semasa proses tersebut dan mempunyai kesan yang sama terhadap elektrod. Tambahan lagi, imej FESEM memaparkan lebih banyak keretakan pada permukaan elektrod selepas kedua-dua rawatan tersebut disebabkan oleh pecahan lapisan PLA, yang meningkatkan kuantiti grafin konduktif dan seterusnya meningkatkan kawasan permukaan elektroaktif elektrod. Akhir sekali, penderiatio elektrokimia PLA/G untuk pengesanan gen BRCA1 telah dibangunkan. Kehadiran rantai tunggal asid deoksiribonukleik (ssDNA) yang dipegun pada permukaan elektrod dibuktikan oleh puncak pengoksidaan ferrosin pada 0.4 V dan puncak guanin pada 0.9 V. Di samping itu, kehadiran lapisan elektrograf asid 6-aminoheksanoik dan prob ssDNA telah disahkan oleh spektroskopi fotoelektron sinar-X (XPS). Tambahan lagi, elektrod terubahsuai ssDNA/3D PLA/G yang dihasilkan melalui kaedah pemegunan kovalen, mempunyai prestasi elektrokimia yang lebih unggul berbanding elektrod kawalan, yang dihasilkan melalui penjerapan fizikal. Pengesanan gen BRCA1 menggunakan elektrod terubahsuai melalui tindak balas hibridisasi adalah memberangsangkan. Walau bagaimanapun, permukaan elektrod terubahsuai ini sangat dipengaruhi oleh penjerapan fizikal molekul ssDNA yang tidak hibrid. Oleh itu, kajian masa depan diperlukan untuk meningkatkan prestasi penderiatio 3D PLA/G BRCA1.

**FABRICATION OF THREE DIMENSIONAL (3D)-PRINTED
ELECTRODES-BASED THERMOPLASTIC CARBON NANOMATERIALS
FOR ELECTROCHEMICAL BREAST CANCER DNA BIOSENSOR**

ABSTRACT

Three-dimensional (3D) printing or additive manufacturing is a promising technology to revolutionise traditional manufacturing methods. Nowadays, numerous studies have utilised 3D printing technology to replace conventional electrodes in the fabrication of electrochemical sensors and biosensors due to its low cost, rapid prototyping, and flexibility in design. The main aim of this study is to explore the 3D-printed electrode's potential as an electrochemical biosensor for breast cancer gene (BRCA1) detection. The first section focuses on the electrochemical performances of 3D-printed polylactic acid/carbon fiber (PLA/CF) electrodes. A novel electrochemical treatment using the differential pulse voltammetry (DPV) technique in hexaammineruthenium (III) chloride (RuHex) solution is proposed. Electrochemical characterisations revealed that the DPV-RuHex electrochemical treatment significantly improved the electrochemical performance of the 3D PLA/CF electrode. Furthermore, field emission scanning electron microscopy (FESEM) micrographs demonstrated that more PLA layers degraded after the treatment, which increased the electrode's electroactive surface area. The second part investigates the effect of DPV treatment in RuHex and sodium hydroxide (NaOH) solutions on the 3D-printed PLA/graphene (PLA/G) electrode. The electrochemical analyses revealed no significant difference between the two treatments. This is because both treatments generate identically strong DPV oxidation signals during the process and have a

similar impact on the electrode. Moreover, FESEM images displayed more cracks on the electrode's surface following both treatments due to PLA layer degradation, which increased conductive graphene availability and thus increased the electrode's electroactive surface area. Finally, the PLA/G electrochemical biosensor for the detection of BRCA1 was developed. The presence of the immobilised single-stranded deoxyribonucleic acid (ssDNA) on the electrode surface was proved by the ferrocene oxidation peak at 0.4 V and a guanine peak at 0.9 V. Furthermore, the electrografted layer of the 6-aminohexanoic acid linker and ssDNA probe were confirmed by X-ray photoelectron spectroscopy (XPS). In addition, the ssDNA/3D PLA/G modified electrode, which was fabricated via covalent immobilisation, has superior electrochemical performance compared to the control electrode, which was created via physical adsorption. The detection of the BRCA1 gene using the modified electrode via hybridisation reaction is promising. However, the modified surface is strongly affected by the physical adsorption of the non-hybridised ssDNA molecules. Thus, future studies are needed to improve the performance of the 3D PLA/G BRCA1 biosensor.

CHAPTER ONE

INTRODUCTION

1.1 Background of the study

Three-dimensional (3D) printing, also known as additive manufacturing, has gained a lot of attention from academics and industries in recent years. 3D printing technology has been used and studied in various research fields, including electrochemical sensing applications [1], food engineering [2], energy [3], and medical applications [4]. 3D printing has received extensive attention due to its advantages such as low cost, biodegradable and recyclable, flexible design options with controlled shape and size, rapid and efficient process, and various materials of choice available to be used [5,6].

3D printing was first found by Hideo Kodama (Figure 1.1) in 1980 and was then developed by Charles Hull in 1984 [7]. It is a process for fabricating desirable structures and products by using a layer-by-layer technique [8].

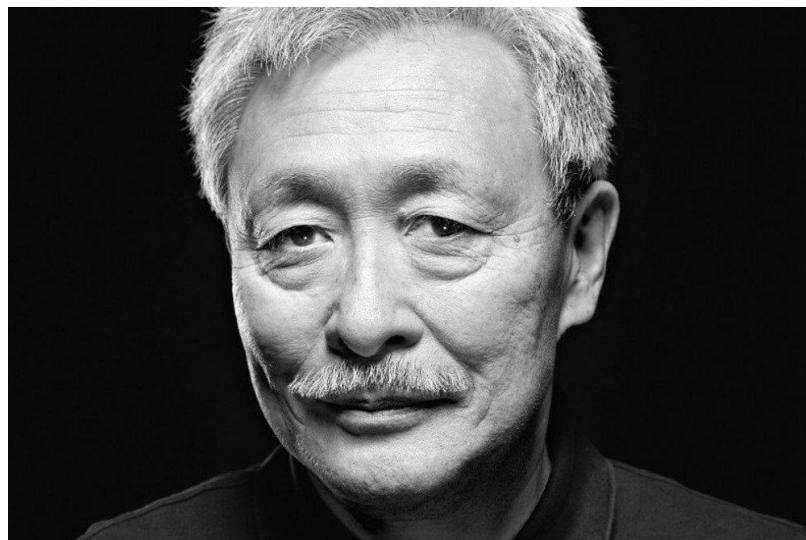


Figure 1.1. Dr. Hideo Kodama is one of the pioneers in 3D printing.

There are several types of 3D printing including material extrusion, vat photopolymerization, material jetting, binder jetting, power bed fusion, direct energy deposition, and sheet lamination [9]. Among them, fused deposition modeling (FDM) is one material extrusion 3D printing example, which is commonly used by academics and researchers nowadays. Figure 1.2 illustrates an example of an FDM 3D printer.



Figure 1.2. Creality CR-6 SE 3D printer is an example of an FDM 3D printer.

The FDM method was invented and developed by Steven Scott Clump in 1989 [10]. The method constructs a designated 3D model by depositing the extruded thermoplastic and other filaments layer by layer onto a stage, commonly known as bed [11]. The filaments are inserted and then moved down by the rollers of the 3D printer to the heated extruder nozzle. The heated filaments are then extruded layer-by-layer to fabricate the designated 3D structure [11]. The standard basic structure of an FDM 3D printer is displayed in Figure 1.3.

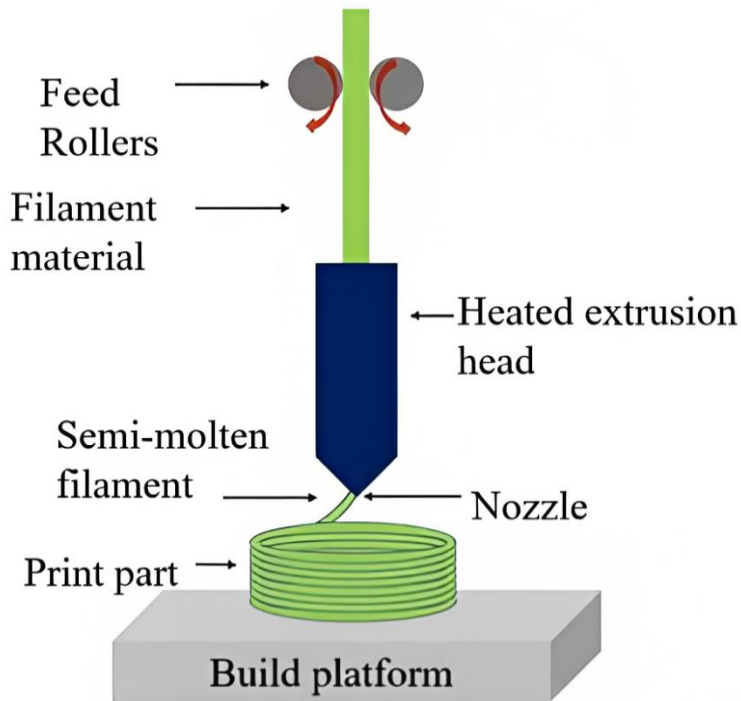


Figure 1.3. The common basic structure of FDM 3D printer.

Before printing the 3D structure, a design must be created first by using computer-aided design (CAD) programs such as Autodesk Tinkercad and Autodesk AutoCAD. Then the design must be converted into .stl (Standard Tessellation Language) file. After that, the design in the .stl file needs to be sliced and converted into .gcode (Geometric Code) file using 3D printing software such as Ultimaker Cura. Finally, the .gcode design file must be transferred into the 3D printer, usually using a removable disk to print the designated 3D product. Figure 1.4 summarises the process of 3D printing. The FDM method is commonly used by researchers because it has several advantages compared to other methods, for example, FDM can fabricate objects from various types of materials such as metals, ceramics and polymers [11]. In addition, it also can print complex parts geometry of the product [12]. Furthermore, other than being easy to obtain and install, the FDM technique usually uses materials that have the characteristics demanded by the researchers, such as materials that have good tolerance to heat [13].

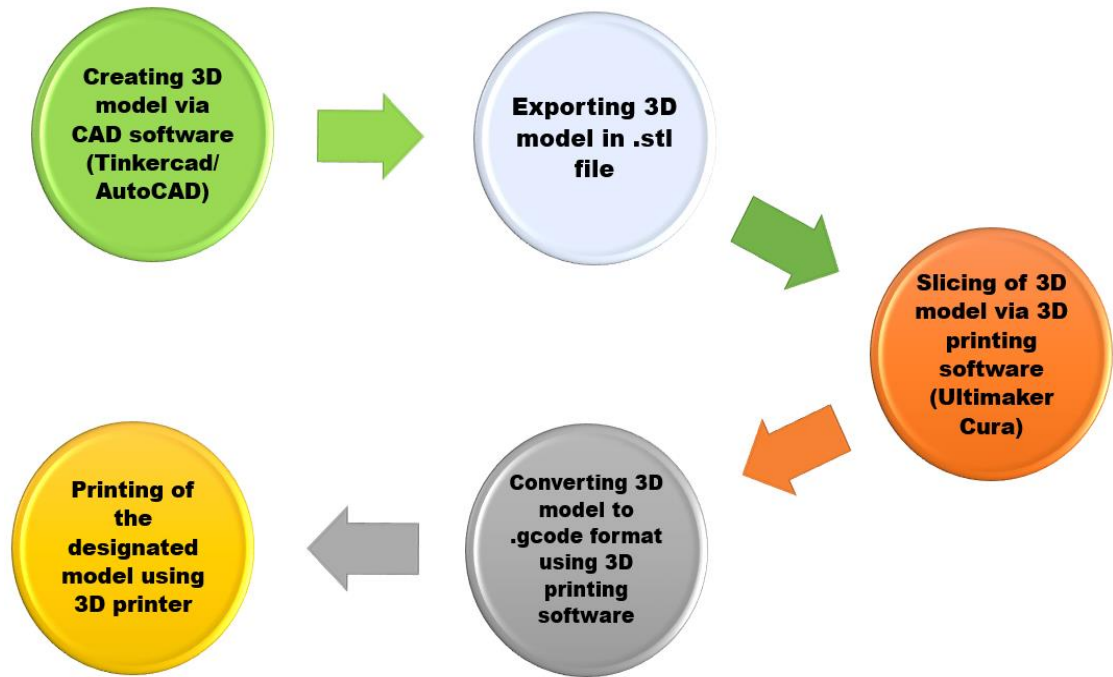


Figure 1.4. Schematic illustration of the FDM 3D printing process.

Filaments used in the process of fabricating 3D models are usually made from polymers such as polylactic acid (PLA) [14], acrylonitrile butadiene styrene (ABS) [15], polyurethane (PU) [16], thermoplastic polyimide (TPI) [17], and nylon [18]. Nevertheless, PLA and ABS, as illustrated in Figure 1.5, are more popular and commonly used as commercialised filaments in FDM 3D printing compared to other filaments. PLA is a biodegradable polymer that derived from its monomer, lactic acid, which can be obtained through the fermentation of sugar and starch [14]. PLA possesses outstanding properties as an FDM 3D printing filament, such as low melting and glass transition temperature, non-adherence to the printing bed surface, and smaller thermal expansion coefficient [19]. Meanwhile, ABS also exhibits characteristics such as low melting temperature [20] and has better resistance to chemicals and moisture [21], which make it an excellent material for FDM 3D printing filament. Nonetheless, PLA is still preferable compared to ABS because it is easier to print, less toxic, and consumes less energy and time to print [22,23].



Figure 1.5. Common thermoplastic PLA and ABS filaments are used in the 3D printing process.

Nowadays, thermoplastic filaments have been modified and reinforced with materials such as metals [24] and carbon nanomaterials [25]. These reinforced materials usually have a significant influence on the printed products' characteristics, such as electrical conductivities and mechanical properties [26]. Carbon fiber [27], graphene [28], carbon nanotubes [29], and carbon black [30] are typical carbon nanomaterials which usually incorporated with PLA and ABS polymers to produce carbon nanomaterial/polymer composite filaments. In essence, carbon nanostructures provide conductive sites, resulting in a three-dimensional model with a conductive surface that can provide active sites for electron transfer processes during redox reactions [31]. Thus, the composite thermoplastic carbon nanomaterial filaments are very well qualified to be used as printing materials for the fabrication and production of electrochemical sensors and biosensors in electrochemical sensing applications. As a result, 3D-printed thermoplastic carbon nanomaterial electrodes by using the FDM technique can offer a great potential to replace conventional electrodes at a lower cost and with greater efficiency.

One of the most important processes for 3D-printed polymer/carbon nanomaterial electrode is the activation step, also known as pre-treatment. This step increases the electrode's electrochemical activity and improves its sensitivity and detection capability. Throughout this step, the polymer layer will be digested and removed, and more underlying conductive carbon nanomaterials will be activated on the 3D-printed electrode surface, resulting in an increase in the electrochemical activities of the 3D-printed electrodes [32]. The activation of 3D-printed electrodes can be achieved by using chemical [33] and electrochemical [34] methods. Chemical activation is accomplished by simply immersing the 3D-printed electrode in chemical agents for a set amount of time. According to Pumera et al. [35], the chemicals utilised in chemical pre-treatment significantly affect the electrochemical performance of the 3D-printed electrode. Meanwhile, the electrochemical activation stage is carried out by immersing the 3D-printed electrode in a chemical solution and applying a specified voltage for a set period of time via electrochemical techniques such as amperometry and cyclic voltammetry. For instance, 3D PLA/carbon black electrodes were electrochemically activated by Munoz et al. [36], by immersing the 3D electrodes in 0.5 M sodium hydroxide solution and applying a potential of +1.4 V followed by -1.0 V, treated for 200 seconds. However, the most effective way for the 3D-printed electrodes to boost its electrochemical behaviour and facilitate faster electron transfer is by performing both chemical and electrochemical activations for the electrode [37].

To date, numerous investigations on 3D-printed electrodes-based carbon nanomaterials have been conducted for electrochemical sensor and biosensor applications. Among several types of filaments, PLA/graphene filaments are commonly used to fabricate thermoplastic 3D-printed electrodes. These 3D-printed electrodes have demonstrated the ability to detect a variety of substances, including

metals [38], biomolecules [39], and even chemical compounds [40]. As electrochemical sensors and biosensors, 3D-printed electrodes are also highly versatile, as they can be adjusted as needed based on the analyte targets of interest. For instance, 3D-printed PLA/graphene electrodes have been modified by electrodeposition of Prussian blue onto the electrodes' surfaces to detect hydrogen peroxide [41]. Consequently, depending on the purpose of the investigations, more research on the modification of the 3D-printed electrode surfaces can be conducted to make them used explicitly in electrochemical applications. In this work, we are interested in studying the potential of the 3D-printed electrodes as an electrochemical DNA biosensor in detecting a breast cancer gene.

Cancer is one of the leading causes of death throughout the world [42]. According to the World Health Organization, there will be around 12 million cancer-related deaths in 2030 [42]. Breast cancer is one of the primary causes of cancer-related mortality among women [43]. Detecting the cancer cells with both fast and efficient methods is one of the vital aspects in preliminary cancer diagnosis [44]. The biomarker is defined as a biological substance found in blood or tissues that indicates a natural or unnatural process or a disease [45]. Therefore, biomarkers allow identifying particular cancers and selecting appropriate treatments, thereby improving the benefit-to-harm ratio of breast cancer screening [46]. There are numerous breast cancer genes such as breast cancer 1 (BRCA1), breast cancer 2 (BRCA2), checkpoint kinase 2 (CHEK2), ataxia-telangiectasia mutated (ATM), and nibrin (NBN) [47]. It has been found that mutations of the BRCA1 gene occur most commonly and significantly increase the risk of developing breast cancer. [48,49]. Consequently, the BRCA1 gene has become an important clinical biomarker for the early detection of breast cancer [50]. In electrochemical DNA biosensing applications in cancer diagnosis, ssDNA molecular

probe is typically immobilised on the surface of the electrodes in order to detect biomarkers of interest [51]. Hence, this work is aiming to explore the potential of 3D-printed electrode as an electrochemical biosensor for the detection of BRCA1.

1.2 Problem statement

Breast cancer is the most prominent cancer among females, resulting in many fatalities. Early detection of breast cancer is crucial for immediate treatment and preventing the disease from worsening. Nowadays, there are some clinical diagnosis tools for breast cancer detection, including mammography, breast ultrasound, and breast magnetic resonance imaging (MRI). Nevertheless, there are some limitations to these techniques. Mammography has been reported to have low sensitivity, especially towards patients under 40 years old and women with higher breast density, high false-positive recall, and may cause excessive exposure to radiation [52–54]. In addition, even though breast ultrasound is non-invasive and safe, it cannot screen many tumors and causes a high rate of false-positive findings, which leads to unnecessary biopsy and testing [55]. Moreover, despite breast MRI having the most heightened sensitivity among the existing clinical modalities for breast cancer screening, the clinical diagnosis expenses for breast MRI are typically high and can become a substantial financial burden for the patient [56]. Consequently, there is an urgent need to develop simple, low-cost, and highly sensitive breast cancer screening and diagnostic tools.

Electrochemical biosensors have a lot of potential for cancer biomarkers detection due to their fast response, high sensitivity, low cost, easy fabrication, simple operation, and mobility [57]. There is a lot of research on developing electrochemical biosensors by employing conventional electrodes and screen-printed electrodes (SPEs)

for cancer biomarkers detection [57–60]. Conventional electrodes, such as glassy carbon and gold electrodes are typically used for biosensors development. However, these types of electrodes are not practical to be used as disposable biosensors since they are not developed for single use. Their surfaces must be regenerated prior to each use, which involves more time and chemicals [61]. Additionally, conventional electrodes are costly to be used as disposable biosensors, making them all the more undesirable. Besides, even though screen-printed electrodes are relatively low-cost and suitable for disposable biosensors, the fabrication of screen-printed electrodes is rigorous, and their designs are not as flexible as those manufactured by 3D printing [62].

3D-printed electrodes have been extensively studied to replace conventional electrodes in electrochemical sensors and biosensors applications [63–65]. 3D-printed electrodes have several advantages, particularly that they can be produced rapidly at a lower cost than conventional electrodes. Furthermore, they can also be designed in a flexible manner depending on the purpose of the research. On top of that, in addition to their cheaper cost, 3D-printed electrodes are also typically made from biodegradable filament composed of PLA, enabling them to be used as disposable biosensors. Due to their significant advantages, 3D-printed electrodes are promising to replace conventional electrodes as biosensors for breast cancer detection. To our knowledge, there is limited publication on 3D-printed electrodes for breast cancer biosensors, particularly in the electrochemical analysis field. Hence, 3D-printed electrodes from carbon fiber and graphene-based PLA filaments were initially fabricated. A novel DPV electrochemical treatment for enhancing the electrochemical performances of the 3D-printed electrodes was also proposed. Finally, this research explored the development of electrochemical DNA biosensors in potentially detecting the BRCA1 gene based on

3D-printed electrodes by covalently immobilising the ssDNA probe to the surface via electrografted amines.

1.3 Research objectives

The objectives of this research are:

1. To fabricate 3D-printed electrodes from PLA/carbon fiber and PLA/graphene filaments using the FDM technique.
2. To evaluate the performances of DPV treated 3D-printed electrodes.
3. To analyse the potential of the fabricated 3D-printed PLA/graphene electrodes towards a breast cancer gene (BRCA1).

1.4 Research overview

This thesis is divided into seven chapters. Chapter One covers the general introduction, the problem statements, and research objectives of the study. Chapter Two discusses the literature review in detail, emphasising the optimisation and applications of 3D-printed electrodes as electrochemical sensors and biosensors, recent electrochemical biosensors based on conventional electrodes for BRCA1 detection, and established clinical methods for early breast cancer diagnosis.

Chapter Three describes the research methodologies used during the project, including the printing and fabrication of the 3D-printed electrodes from PLA/graphene and PLA/carbon fiber filaments, the chemical and electrochemical activations of the electrodes, the characterisation techniques used, and the synthesis

and evaluation of the 3D-printed PLA/graphene electrodes for the detection of BRCA1.

The main objective of this research is to modify a 3D-printed electrode based on PLA/carbon nanomaterial filaments to detect a breast cancer biomarker of BRCA1 gene. In order to accomplish this, the electrode must first be fabricated in-house. In Chapter Four, 3D-printed electrodes made from PLA/carbon fiber filament have been printed and fabricated. A novel electrochemical treatment by utilising the DPV technique has been proposed to improve the electrochemical performances of the electrode. Furthermore, the electrochemical and morphological characterisations of the 3D-printed PLA/carbon fiber electrode have been carried out.

Chapter Five reports on the effect of the DPV treatment by using different solutions (RuHex and NaOH) on 3D-printed PLA/graphene electrodes. Electrochemical performance of the electrodes after both treatments were examined using electrochemical characterisations such as CV and EIS techniques. Furthermore, the surface morphologies of the 3D-printed PLA/graphene electrodes before and after being subjected to both treatments were studied by using FESEM. In-depth analyses were carried out to compare the differences between both DPV treatments.

Chapter Six reports on the developed electrochemical DNA biosensor-based 3D PLA/graphene electrodes. The ssDNA/3D PLA/graphene modified electrode was fabricated via electrografting of 6-aminohexanoic (6-ACH) acid and immobilisation of BRCA1 ssDNA probe on the surface of the electrode. The electrochemical performances of the ssDNA probe was evaluated using the DPV technique, and XPS analyses were conducted to study and characterise the surface changes in chemical bonding of the modified surface. In addition, the ssDNA/3D PLA/G modified electrode hybridisation assays were analysed by exposing the ssDNA/3D PLA/G

modified electrode to complementary ssDNA (target) and non-complementary (NC) ssDNA.

Finally, Chapter Seven summarises all research findings and provides recommendations for future works of the study.

CHAPTER TWO

LITERATURE REVIEW

In recent years, numerous studies have been performed on the enhancement and optimisation of carbon nanomaterials/polymer filament-based 3D-printed electrodes. The research also include the impact of printing, the influence of carbon nanomaterials contents, and the role of activation steps on the 3D-printed electrodes. 3D-printed electrodes have also been studied for many applications, including as electrochemical sensors and biosensors. Hence, the studies related to the optimisation and applications of 3D-printed electrodes will be discussed in the next part.

2.1 The effect of printing on the electrodes' electrochemical behaviour

The effect of printing and orientation of the 3D electrodes on their electrochemical behaviours has been demonstrated by Patel et al. [66]. They have printed 3D ABS/carbon black (ABS/CB) electrodes in two printing directions, which were vertical and horizontal directions. The authors reported that printing in a horizontal direction produced two types of electrode surfaces, horizontal printed smooth surface (HPSS) and horizontal printed rough surface (HPRS). This is due to the fact that during horizontal printing, the first layer was thinner than the main layer, resulting in a smooth HPSS surface at the bottom of the electrode. In the meantime, when more infill and layers are printed, a rougher surface is generated at the top of the electrode, resulting in the formation of HPRS. The voltammetric electrochemical responses of the HPSS, HPRS, and vertical printed (VP) electrodes were evaluated in 1 mM ferrocene carboxylic acid and 1 mM serotonin hydrochloric acid redox

solutions. The voltammetric results indicated that the VP electrode displayed the best electrochemical response with the highest current generation as compared to both HPSS and HPRS electrodes. Furthermore, the EIS results revealed that the VP electrode demonstrated the lowest charge transfer resistance (R_{ct}) values when compared to both horizontally printed electrodes. The authors concluded that printing in vertical directions provides superior and enhanced electrochemical performance compared to printing in horizontal directions. This is because the internal structure of the vertical print layers is arranged in a manner that follows the conductive pathways from the electrical connection to the solution interface.

In a different study, Patel et al. have also investigated the printing and orientation effect on the electrochemical behaviours of 3D-printed PLA/carbon black electrode [67]. They have printed 3D electrodes from PLA/carbon black (PLA/CB) filament with layer thickness ranging from 0.1 to 0.4 mm in two different printing orientations, vertical and horizontal states, as illustrated in Figure 2.1. The electrochemical performances of the 3D PLA/CB electrodes were characterised by using CV in 1 mM hexaammineruthenium (III) chloride in potassium chloride and 1 mM serotonin in Krebs' buffer solution, as well as EIS in ferricyanide/ferrocyanide redox couple ($[\text{Fe}(\text{CN})_6]^{3-/4-}$).

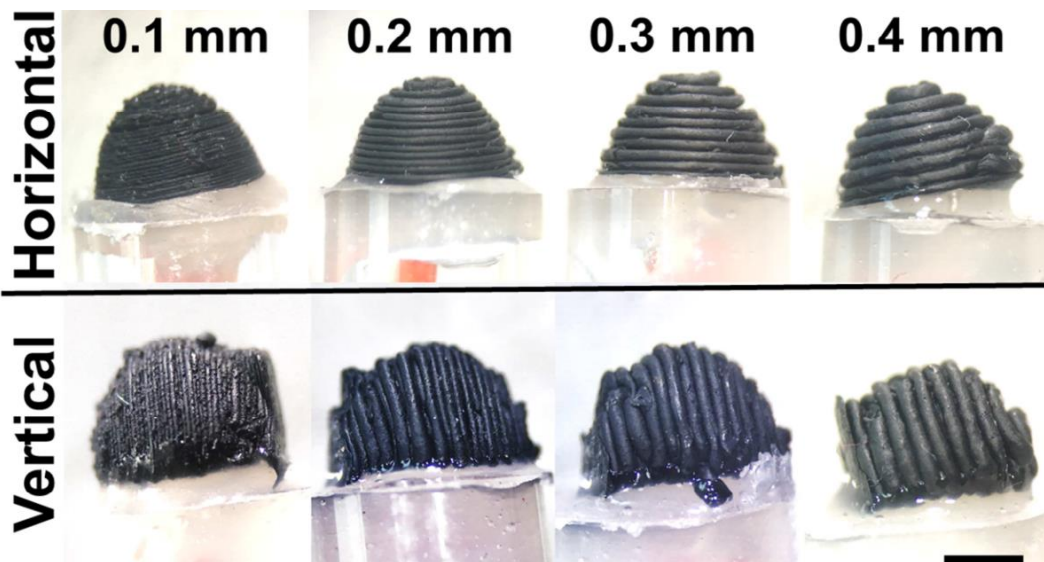


Figure 2.1. 3D PLA/CB electrodes were printed in different thicknesses of 0.1 to 0.4 mm with horizontal and vertical orientations [67].

From CV data, the 3D PLA/CB electrodes printed in vertical orientation and with the low thickness (0.1 and 0.2 mm) exhibited improved electrochemical performances. Furthermore, such 3D PLA/CB electrodes displayed lower charge transfer resistance (R_{ct}) compared to thicker 3D PLA/CB electrodes printed in a horizontal state. The authors implied that printing in a vertical position reduced the influence of air voids, hence reducing the resistance within filaments during the printing phase. The researchers also suggested that PLA/CB structures printed in a vertical orientation are more compact and ordered than those printed in a horizontal orientation because the composition of CB particles is greater than that of PLA, causing CB to be more oriented towards the middle. At the same time, PLA is pushed to the sides. Thus, the authors concluded that 3D-printed PLA/CB electrodes printed in a vertical orientation with a small thickness layer provide the best electrochemical performance and conductivity of the electrodes.

2.2 The effect of carbon nanomaterials contents on the 3D-printed electrodes

Picking the appropriate filament is one of the most critical aspects of 3D printing electrodes, particularly for electrochemical sensing applications. According to a number of studies, the composition of carbon nanomaterials within the filament plays a crucial impact on printed specimens. For instance, a study on mechanical and electrical characteristics utilising different carbon nanotubes (CNT) compositions within thermoplastic polyimide (TPI) has been carried out by Wu et al. [68]. They prepared TPI filaments containing different CNT weight (wt.) percentages of 1%, 3%, 5%, 7%, 9% and then the filaments were used for 3D printing using FDM method, as displayed in Figure 2.2. According to the authors, the bending and tensile strengths of the printed specimens decreased as the CNT content increased. The authors also observed that when the CNT content in the filaments increased, the conductive resistivity of the 3D specimens decreased. The conductive percolation threshold of the 3D TPI/CNT specimens was then determined to be 3% based on the conductive resistivity plot. This study demonstrated that the composition of carbon nanomaterials in the polymer matrix significantly affected the filament's properties, particularly its electrical and mechanical capabilities.

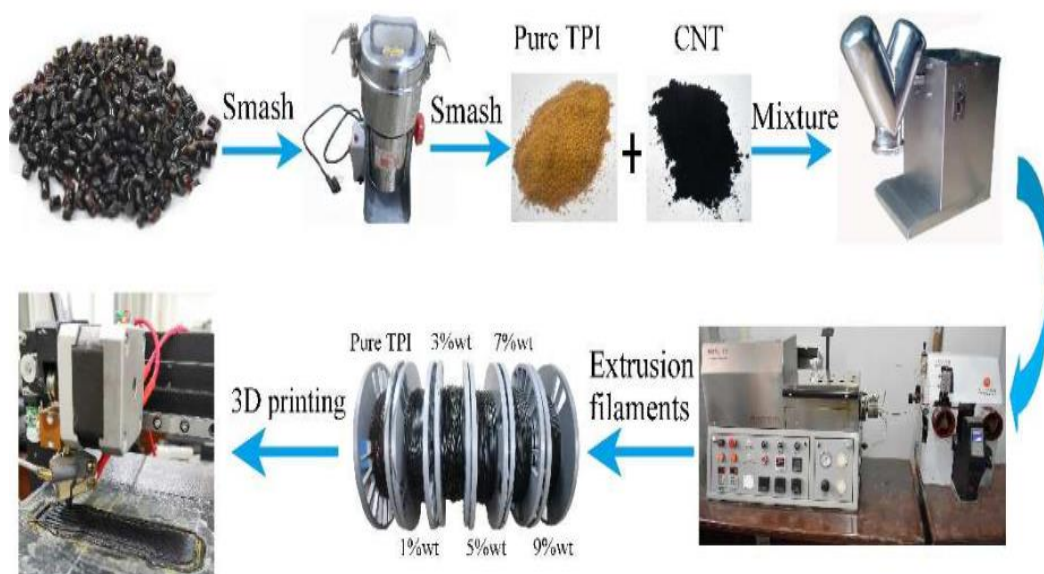


Figure 2.2. Preparation of TPI/CNT filament containing different wt% of CNT [68].

In another study [69], Banks and co-workers fabricated 3D-printed electrodes by using PLA/nanographite (NG) filament with varying the composition of NG within the PLA matrix. They have utilised different wt. percentage of NG (1, 5, 15, 20, 25, and 40 wt%) to produce PLA/NG filaments for 3D electrode printing purposes. Afterward, the electrochemical and physiochemical properties of the printed electrodes were assessed. The percolation study revealed that PLA/NG filaments with greater than 20 wt% NG content demonstrated effective percolation and superior conductivity, as depicted in Figure 2.3. However, according to the authors, NG amounts of more than 25 wt% resulted in the filament that was brittle due to the insufficient PLA thermoplastic content, and the printing process was not able to take place. Therefore, the authors utilised 3D-printed electrodes made from a filament containing 25 wt% NG for future study characterisation and application.

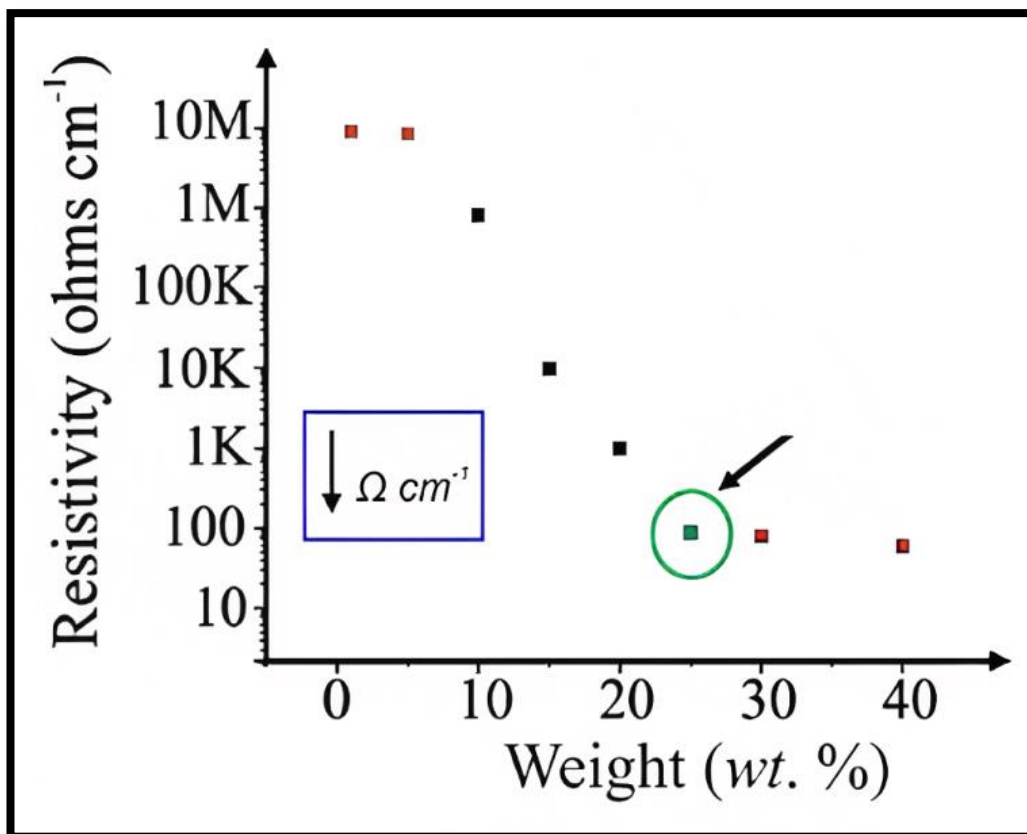


Figure 2.3. Resistivity against NG content plot, demonstrating effective percolation for NG content more than 20% which results in higher conductivity [69].

For electrochemical evaluation, 3D PLA/25%-NG electrodes displayed graphitic behaviour and good electrochemical response for the tested redox analytes. Moreover, the 3D PLA/25% -NG electrodes were utilised to detect lead (II) and cadmium (II) ions using the square wave voltammetry (SWV) technique. Based on the study of SWV profiles, the 3D electrodes identified both metals and displayed linearity over the concentration range ($R^2=0.98$ for lead (II) and $R^2=0.99$ for cadmium (II)). This study demonstrated yet again that nanomaterial content substantially affected the filament's characteristics.

2.3 Chemical and electrochemical activation studies on 3D-printed electrodes

For past years, various studies have been carried out on the chemical and electrochemical activation of 3D-printed PLA/carbon nanomaterials electrodes. Pumera and his co-workers have investigated the effect of different solvents used in the chemical activation of 3D-printed PLA/graphene (3D PLA/G) electrodes [35]. The 3D PLA/G electrodes have been immersed and sonicated in different types of solvents, consisting of polar protic solvents (ethanol, methanol, and deionised water) and polar aprotic solvents (dimethylformamide (DMF) and acetone). Then, the 3D PLA/G electrodes were washed with deionised water and left dried for one night. From the CV results shown in Figure 2.4A, both polar aprotic solvents have a more significant effect on the electrochemical performance of 3D PLA/G electrodes compared to all polar protic solvents. Both CVs of 3D PLA/G electrodes activated in DMF and acetone show well-defined peaks of $[\text{Fe}(\text{CN})_6]^{3-/4-}$. Despite the CVs for all polar protic solvents not showing the redox peaks clearly, the currents for all the CVs showed an increased pattern compared to unactivated 3D PLA/G electrodes, as illustrated by Figure 2.4B, indicating that the surface of 3D PLA/G electrodes have been altered by polar protic solvents.

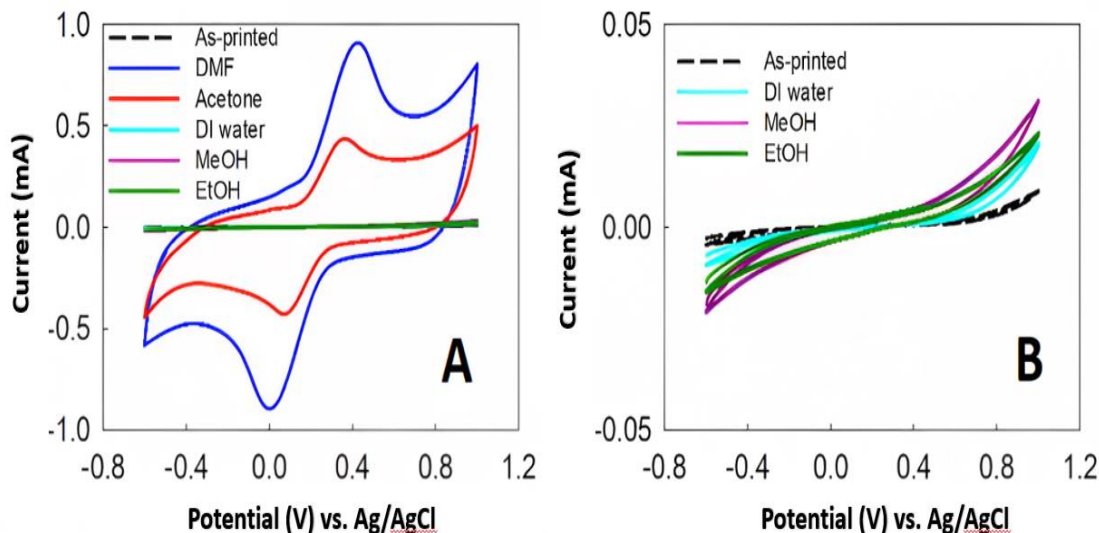


Figure 2.4. (A) and (B) showing cyclic voltammograms in $[\text{Fe}(\text{CN})_6]^{3-/4-}$ solution of 3D PLA/G electrodes after chemically activated with different solvents [35].

Furthermore, the authors reported that the CV peak separation of 3D PLA/G electrode activated in acetone (296 mV) was lower than that of 3D PLA/G activated in DMF (416 mV). This indicated that the 3D PLA/G electrode activated in acetone has faster heterogeneous electron transfer, due to the rougher surface, compared to the 3D PLA/G electrode activated in DMF. However, the authors found that 3D PLA/G electrode activated in DMF gave the best supercapacitor behaviour compared to acetone-activated 3D PLA/G. Finally, the authors suggested that acetone should be used for future studies of 3D PLA/G electrodes in electrochemical applications because acetone is less harmful than DMF and still has excellent activation capabilities. Nevertheless, some studies [70], including studies conducted by Pumera and his co-workers [32], chemically activated 3D PLA/G electrodes by immersing the electrodes in DMF for 10 minutes, where 10 minutes is the optimum immersion time for 3D PLA/G in DMF.

Besides chemical activation, electrochemical activation also plays an important role in increasing the electrochemical behaviour of 3D-printed PLA/carbon

nanomaterials. Firstly, Richter et al. fabricated 3D PLA/CB electrodes by using the FDM method for the detection analysis of dopamine [71]. Then, the authors reported that the 3D PLA/CB electrodes delivered poor results due to poor-defined oxidation peaks for the tested compounds (ascorbic acid, uric acid, dopamine, and ferricyanide/ferrocyanide redox couple). Thus, the authors carried out electrochemical activation for 3D PLA/CB in a sodium hydroxide (NaOH) solution using cyclic voltammetry and amperometry techniques. Several parameters of the electrochemical activation were tested. The best results obtained for the electrochemical activation of 3D PLA/CB electrode by applying amperometric technique with sequence potential of +1.4 V for 200 seconds and -1.0 V for 200 seconds in 0.5 M NaOH solution. After the electrochemical activation, the 3D PLA/CB electrodes' electrochemical performances significantly improved as the current intensity increased and the peak separation decreased for the tested analytes. Furthermore, from SEM analyses, the availability of carbon black nanoparticles increases after the electrochemical activation, indicating an increased the electrochemical surface area of 3D PLA/CB electrodes. Finally, the 3D PLA/CB electrodes successfully detected dopamine with limit of detection of 0.1 μ M.

Besides, Pumera and colleagues also fabricated 3D-printed PLA/nanocarbon (3D PLA/nC) and 3D PLA/CB electrodes for activation study of the electrodes [72]. To electrochemically activate both 3D electrodes, Pumera and his co-workers applied a fixed 2.5 V potential for 1000 seconds against silver/silver chloride (Ag/AgCl) reference electrode in phosphate buffer saline solution (pH 7.2). Intriguingly, they did their research to develop a new chemical activation method, as an alternative to the previous method, which is by using DMF. In this study, they have tested different chemical activation solvents; reducing agents of sodium borohydride, hydrazine (with deionised water), lithium aluminium hydride (with tetrahydrofuran) and ascorbic acid,

and oxidising agent of hydrogen peroxide (with deionised water). Based on the outcome, sodium borohydride has been discovered to be the best chemical activation solvent for both 3D-printed electrodes and produce activated electrodes with electrochemical performances comparable to those achieved using the standard DMF approach, as shown in Figures 2.5 and 2.6. The authors have reported that 1 M of sodium borohydride and 30 min of immersion time are the optimal parameters for this study.

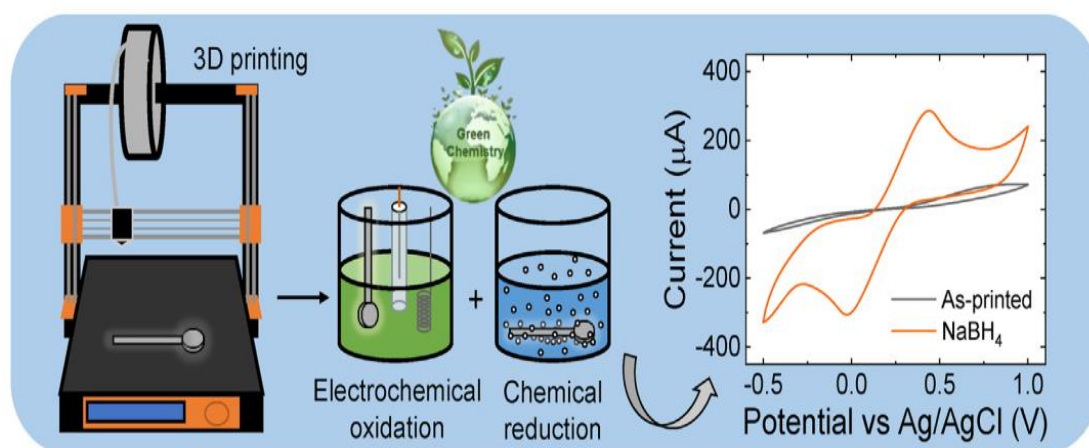


Figure 2.5. Preparation of 3D-printed electrodes with electrochemical activation and chemical activation using sodium borohydride. The cyclic voltammograms indicated the electrodes' redox activity before and after activation in $[\text{Fe}(\text{CN})_6]^{3-/4-}$ solution [72].

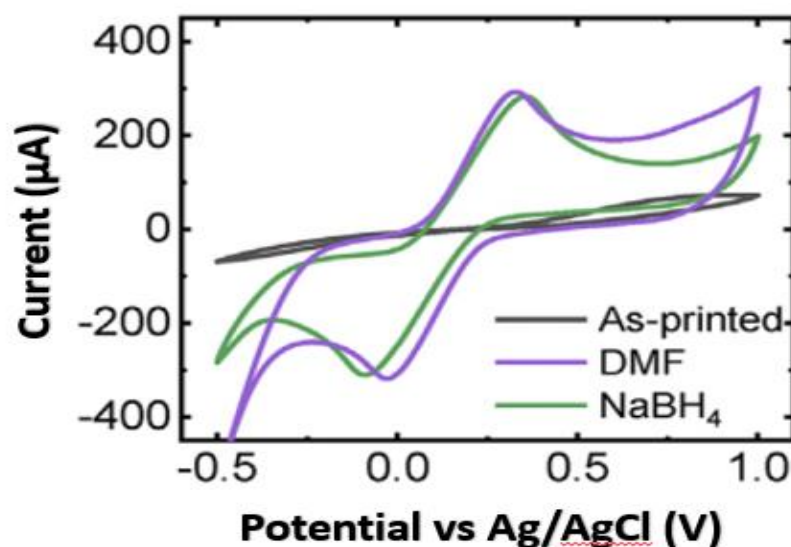


Figure 2.6. Cyclic voltammograms of the 3D-printed nanocarbon electrodes before and after activating with DMF and sodium borohydride (NaBH_4) solutions [72].

NaBH₄ has proven to enhance the electrochemical activity (increase current density and reduce peak separation) of both 3D PLA/nC and 3D PLA/CB electrodes by removal of the PLA layer which increasing and exposing more carbon nanoparticles of both 3D electrodes to the [Fe(CN)₆]^{3-/4-} redox couple. Rather than using toxic organic solvent such as DMF, this study has provided an alternative for the eco-friendly chemical activation approach by using sodium borohydride. Table 2.1 summarises different approaches of the activation methods reported in the literature for 3D-printed electrodes.

Table 2.1: Summary of activation methods of the 3D-printed electrodes with their respective applications.

Type of 3D-printed electrodes	Activation methods	Application of the 3D-printed electrodes
3D-printed PLA/graphene electrodes [73]	<ul style="list-style-type: none"> - Chemical activation in 3 M NaOH for 30 minutes - Electrochemical activation in 0.1 M PB solution (pH 7.4) by applying +1.8 V for 900 seconds followed by CV for one cycle at 0.0 to -1.8 V potential range and at scan rate of 50 mV s⁻¹ 	Electrochemical detection of L-methionine in human serum samples
3D-printed PLA/graphene electrodes [74]	<ul style="list-style-type: none"> - Chemical activation in DMF for 10 minutes - Electrochemical activation in 0.1 M PB solution (pH 7.4) by applying +1.8 V for 900 seconds followed by CV for one cycle at 0.0 to -1.8 V potential range and at scan rate of 50 mV s⁻¹ 	Electrochemical detection of L-cysteine in human serum samples

3D-printed PLA/carbon black electrodes [75]	<ul style="list-style-type: none"> - Mechanical polishing with sandpaper sheets and sulphite paper - Electrochemical activation in 0.5 M NaOH by amperometry technique at a potential of +1.4 V followed by -1.0 V for 200 seconds. 	Determination of sulfanilamide in breast milk, otologic solution, and synthetic urine samples
3D-printed PLA/graphene electrodes [40]	<ul style="list-style-type: none"> - Chemical activation in DMF for 10 minutes 	Detection of chlorophenols and nitrophenols in aqueous solutions
3D-printed PLA/graphene electrodes [76]	<ul style="list-style-type: none"> - Chemical activation in DMF for four hours 	Electroplating of 3D-printed electrodes with copper and nickel, and electrochemical detection of glucose and sucrose
3D PLA/carbon black electrodes [77]	<ul style="list-style-type: none"> - Mechanical polishing with sandpaper - Electrochemical activation in 0.5 M NaOH by applying a potential of +1.4 V followed by -1.0 V for 200 seconds. 	Simultaneous detection of lead and copper in tap water and liquid fuel samples
3D-printed PLA/carbon black electrodes [78]	<ul style="list-style-type: none"> - Mechanical polishing with abrasive paper - Electrochemical activation in 0.5 M by applying a potential of +1.4 V followed by -1.0 V for 200 seconds. 	Determination of hydroxychloroquine in tap water and pharmaceutical samples
3D-printed PLA/carbon black electrodes [79]	<ul style="list-style-type: none"> - Photo-Fenton method activation by adding 100 μL solution consisting of Fe(II) and hydrogen peroxide (15%) to the electrodes and then exposing the electrodes to UV/Vis light for 5 minutes - Electrochemical activation in 6 M acetic acid (pH 2.1) by applying +1.8 V potential for 200 seconds 	Detection of midazolam in drinks, uric acid in biological fluids and metals in the aerosol atmosphere